



# MODELING AND SIMULATION OF A MEDIUM VOLTAGE CASCADED H-BRIDGE M-LEVEL INVERTER DRIVE SYSTEM USING FUZZY CONTROLLER

<sup>1</sup>PATHI HOLY RANI, <sup>2</sup>B.CHANDRA SEKHAR REDDY

<sup>1</sup>M.Tech, ANURAG Group of Institutions(Formerly known as CVSR College of Engineering(Autonomous))Affiliated to JNTUH, Hyderabad, Telangana, India.

<sup>2</sup>Assistant Professor, ANURAG Group of Institutions(Formerly known as CVSR College of Engineering(Autonomous))Affiliated to JNTUH, Hyderabad, Telangana, India.

**ABSTRACT-** A dynamic load model of a medium voltage cascaded H-bridge multi-level inverter drive and an induction motor system is presented in this paper. In high-power applications medium voltage drives (MVDs) are commonly used and show significant impact on the overall system dynamics due to their large size and high power demand. In this paper, we are using the fuzzy controller compared to other controllers i.e. The fuzzy controller is the most suitable for the human decision-making mechanism, providing the operation of an electronic system with decisions of experts. To overcome this problem, in this paper the dynamic load model for the medium voltage cascaded H-bridge multi-level inverter drive and induction motor systems, which is suitable for power system dynamic studies, is proposed. Both voltage and frequency dependence are considered in the model. The accuracy of the model is verified by simulation results. A sensitivity study is conducted to evaluate the impact of the model parameter variation on dynamic response characteristics. By using the simulation results we can analyze the proposed method.

**INDEX TERMS:** Cascaded H-bridge multi-level inverter, frequency dependence, Fuzzy logic controller, load model, medium voltage drives (MVDs), power system dynamic studies, voltage dependence.

## I. INTRODUCTION

Medium voltage drives (MVDs) are commonly used in high power applications and show significant impacts on the overall system dynamics due to their large size and high power demand. Multilevel inverters have been attracting because of increased power ratings, better harmonic performance and optimized electromagnetic interference (EMI) emission that can be archived with multiple DC levels that are a synthesis of the output voltage waveform. It has been recognized for more than two decades that representations of power system loads for dynamic performance analysis can have

significant impact on power system stability. As power systems are designed and operated with a lower stability margin, adequate load models are of major importance [1], [2]. VFDs are widely used in various industrial sectors. The modeling needs for such devices become more important as their penetration level in power systems increases over time. Power electronic devices including VFDs were extensively investigated for modeling in the past.

In power systems, a load model is a mathematical representation of the relationship between the bus voltage (magnitude and frequency) and the real and reactive power owing into the bus; There are two types of load models: static and dynamic load models. The static load model involves algebraic equations. It is essentially used for static load components, such as resistive and lighting loads.

Two types of dynamic load models are proposed for large industrial loads in [12]: a transfer function model, and a composite load model (an induction motor in parallel with a shunt static load). The dynamic load model expressed by a transfer function for power grid is recommended in [13] and [14], which appears to be a well-accepted dynamic load model format.

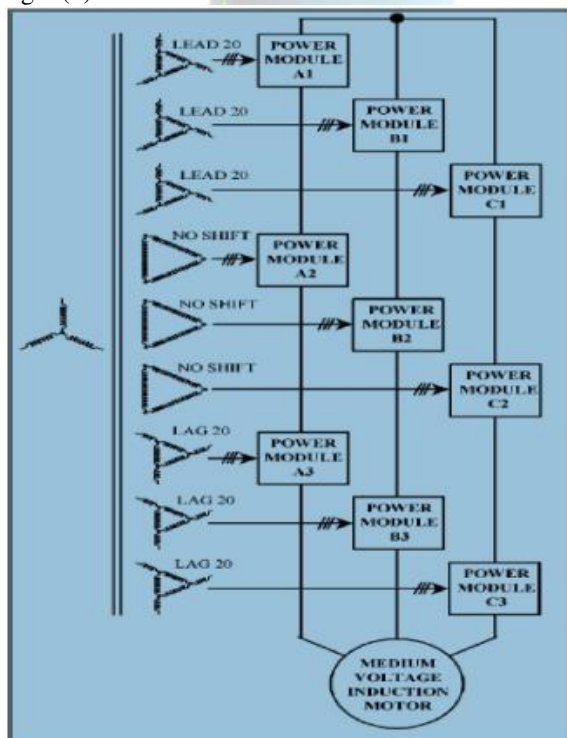
In real life, VFDs will trip out of line under large disturbances and will be able to ride-through when experiencing small disturbances. The equivalent load model is intended for the ride-through case related to small disturbances, and thus, it can be treated as a small-signal stability problem. Therefore, the equivalent load model for motor drive systems can be developed using the linearization approach and expressed by transfer functions. Developing adequate dynamic load models for medium voltage motor drive systems is essential for power system stability studies.

## II. DYNAMIC LOAD MODEL DEVELOPMENT

The medium voltage cascaded H-bridge multi-level inverter drives are one of the topologies for very high power applications. The drive is constructed using a series of low voltage power modules. Usually, 9 power modules form an 18-pulse system, and 12 power modules form a 24-pulse system at the drive input.

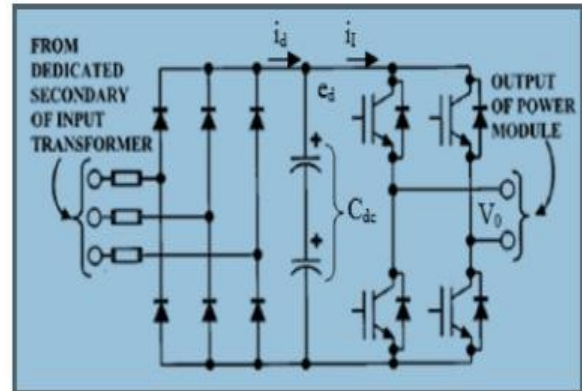
The topology of a 9-power-module 18-pulse medium voltage drive can be found. For these 18-pulse drives, there are three power modules in a phase leg, and the drives can produce as much as 1,440 V line-to-neutral, or 2,494 V line-to-line at the output. The topology of a nine-power-module 18-pulse medium voltage drive and an induction motor system is shown in Fig. 1(a).

Each power module is a static pulse-width-modulated (PWM) power converter. It consists of a three-phase full bridge diode converter, a DC link, and a single-phase full bridge inverter. The schematic diagram of each power module is shown in Fig. 1(b).



(a)

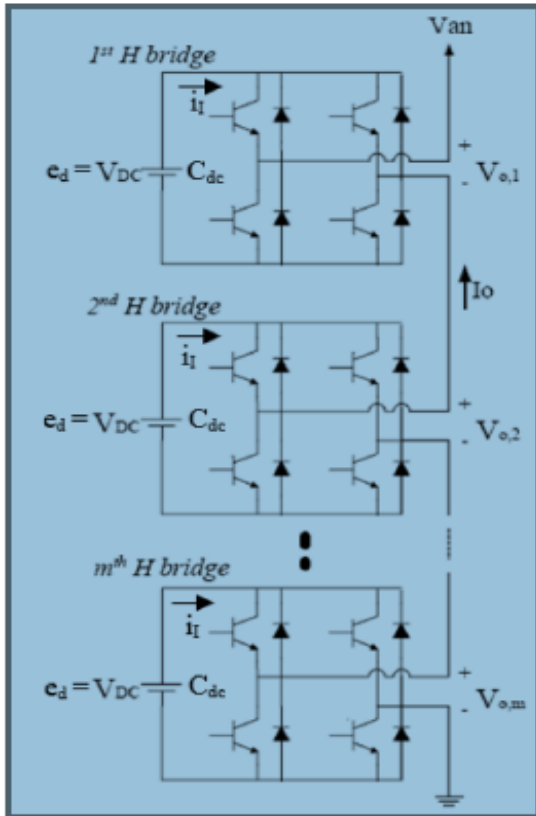
FIGURE.1 Eighteen-pulse cascaded H-bridge M-level inverter motor drive system: (a) the topology of a nine-power-module drive.



(b)

FIGURE.1 Eighteen-pulse cascaded H-bridge M-level inverter motor drive system: (b) the schematic diagram for each power module

The three-phase full bridge diode converter is exactly the same as the low voltage 6-pulse drive, which is capable of receiving input power from one of the phase-shifting transformer secondary windings at 480 V, 50/60 Hz, and charging a DC link capacitor to about 600 V dc voltage. The outputs of multiple single-phase inverters are connected in series, feeding one phase of an induction motor [20]. The outputs of the single-phase full bridge inverters connected to phase a of an induction motor are shown in Fig. 1(c).



(c)

FIGURE.1 Eighteen-pulse cascaded H-bridge M-level inverter motor drive system: (c) outputs of the single-phase full bridge inverters connected to phase a of an induction motor.

### A. Mathematical model of converter and dc link for each power module and induction motor

In this paper, the mathematical derivation of the dynamic load model for a medium voltage cascaded H-bridge multi-level inverter motor drive system starts from each low voltage power module.

For the low voltage power modules connected to the transformer secondary windings without a phase-shifting (i.e., the phase-shifting angle is equal to 0), differential equations for the converter and the DC link are the same as that used for the low-voltage voltage source inverter drive.

### B. Mathematical model of the inverter for each power module

It is verified in this study that the DC link voltage from the diode converter connected to the transformer secondary winding with a phase-shifting angle not equal to 0 are exactly the same as that from the diode converter connected to the transformer

secondary winding with a phase-shifting angle equal to 0. Therefore, the phase shift angle of the transformer winding does not affect the DC link voltage from the converter in each power module.

The output voltage from the single-phase full bridge inverter for each power module can be determined as follows:

$$V_0 = de_d \quad (1)$$

where  $V_0$  is the output voltage from each power module,  $d$  is duty cycle,  $e_d$  is the DC link voltage before the inverter. The line to neutral voltage of the induction motor at phase a  $V_{an}$  can be determined as follows:

$$V_{an} = \left(\frac{n_{pulse}}{6}\right) de_d \cos(\omega_s t) \quad (2)$$

where,  $n_{pulse}$  is the pulse number of the MVD,  $\omega_s$  is the stator electrical field angular velocity in rad/s for the induction motor.

For eighteen-pulse MVD, three-power-module per phase are connected to the induction motor. The pulse number  $n$ -pulse is assigned as follows:

$$n_{pulse} = 18 \quad (3)$$

The voltages at phases b and c can be determined as phase a by the following equations:

$$V_{bn} = \left(\frac{n_{pulse}}{6}\right) de_d \cos\left(\omega_s t - \frac{2\pi}{3}\right) \quad (4)$$

$$V_{cn} = \left(\frac{n_{pulse}}{6}\right) de_d \cos\left(\omega_s t + \frac{2\pi}{3}\right) \quad (5)$$

The three phase line-to-neutral voltages of the induction motor in the  $abc$  frame are converted to the  $dq0$  frame by

$$V_{qs} = \left(\frac{n_{pulse}}{6}\right) de_d \quad (6)$$

$$V_{ds} = 0 \quad (7)$$

where  $V_{qs}$  is the q-axis terminal voltage of the induction motor, and  $V_{ds}$  is the d-axis terminal voltage of the induction motor.

The real power supplied to the induction motor  $P_{ac\_IM}$  can be expressed as follows:

$$\begin{aligned} P_{ac\_IM} &= \frac{3}{2} (V_{ds} i_{ds} + V_{qs} i_{qs}) = \frac{3}{2} V_{qs} i_{qs} \\ &= \frac{3}{2} * \left(\frac{n_{pulse}}{6} de_d\right) i_{qs} = \left(\frac{n_{pulse}}{4}\right) de_d i_{qs} \quad (8) \end{aligned}$$

where  $i_{ds}$  and  $i_{qs}$  are the d-axis and q-axis components of the stator current of the induction motor, respectively.

The total DC power at the DC link for all power modules,  $P_{dc}$ , corresponding to the real power supplied to the induction motor can be calculated as follows:

$$P_{dc} = \left(\frac{n_{pulse}}{2}\right) P_{dc\_per\_module} = \left(\frac{n_{pulse}}{2}\right) e_d i_1 \quad (9)$$

where,  $i_1$  is the DC link current entering the inverter inside each power module.



Ignoring losses at the inverters inside power modules, the subsequent equation is satisfied as follows:

$$P_{ac\_IM} = P_{dc} \quad (10)$$

Based on (8)-(10), we have

$$\left(\frac{n_{pulse}}{4}\right) de_d i_{qs} = \left(\frac{n_{pulse}}{2}\right) e_d i_1 \quad (11)$$

The DC link current entering the inverter  $i_l$ , the DC link current after the converter/rectifier  $i_d$ , the DC link voltage before the inverter  $i_l$ , and the capacitance of the DC link capacitor  $C_{dc}$  have the relationship as follows:

$$i_l = i_d - C_{dc} \frac{de_d}{dt} \quad (12)$$

Substitute (12) in (11), we have

$$\frac{1}{2} de_d i_{qs} = e_d \left( i_d - C_{dc} \frac{de_d}{dt} \right) \quad (13)$$

The q-axis component of the stator current can be determined from (13) as follows

$$i_{qs} = \frac{2i_d}{d} - 2C_{dc} \left( \frac{de_d}{dt} \frac{1}{d} \right) \quad (14)$$

Linearize (14), the following can be determined as follows:

$$\Delta i_{qs} = \frac{2}{d_0} \Delta i_d - \frac{i_{qs0}}{d_0} \Delta d - \frac{C_{dc}}{d_0} S \Delta e_d \quad (15)$$

where S is the Laplace Transform variable.

### C. Mathematical model of the control scheme

The control system used in load modeling of the medium voltage motor drive system is the closed-loop voltage per Hz control. If a different control method is used, equations for control systems need to be adjusted accordingly. Reference [11] provides information on the voltage control method for the duty-cycle modulator. The goal is to obtain the appropriate duty cycle(s) and the converter reference frame position in order to achieve a desired fast average synchronous reference frame direct- and quadrature-axis voltages [11].

$$\begin{bmatrix} v_{qs}^e \\ v_{ds}^e \end{bmatrix} = \begin{bmatrix} \cos \theta_{ce} & \sin \theta_{ce} \\ -\sin \theta_{ce} & \cos \theta_{ce} \end{bmatrix} \begin{bmatrix} v_{qs}^c \\ v_{ds}^c \end{bmatrix} \quad (16)$$

where  $\theta_{ce}$  is angular displacement of the converter reference frame from the synchronous reference frame, and

$$\theta_{ce} = \theta_c - \theta_e \quad (17)$$

Replacing  $v_{qs}^e$  with the commanded value  $v_{qs}^{e*}$ , replacing  $v_{ds}^e$  with the commanded value  $v_{ds}^{e*}$ , and replacing  $v_{qs}^c$  and  $v_{ds}^c$  with the average values expression by (6) and (7), we have

$$\begin{bmatrix} v_{qs}^{e*} \\ v_{ds}^{e*} \end{bmatrix} = \begin{bmatrix} \cos \theta_{ce} & \sin \theta_{ce} \\ -\sin \theta_{ce} & \cos \theta_{ce} \end{bmatrix} \begin{bmatrix} v_{qs}^c \\ v_{ds}^c \end{bmatrix} \quad (18)$$

$$= \begin{bmatrix} \cos \theta_{ce} & \sin \theta_{ce} \\ -\sin \theta_{ce} & \cos \theta_{ce} \end{bmatrix} \begin{bmatrix} \frac{n_{pulse}}{6} de_d \\ 0 \end{bmatrix} \quad (19)$$

From (18), the following can be obtained:

$$d = \frac{\sqrt{(v_{qs}^{e*})^2 + (v_{ds}^{e*})^2}}{\left(\frac{n_{pulse}}{6}\right) de_d} \quad (20)$$

The block diagram of the closed-loop voltage per Hz control scheme for the eighteen-pulse cascaded H-bridge M-level inverter motor drive system is shown in Fig. 2.

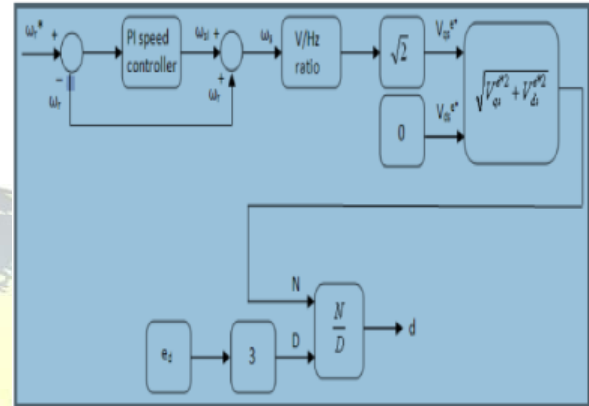


FIGURE.2 Closed-loop voltage per Hz control scheme for the eighteen-pulse cascaded H-bridge M-level inverter motor drive system.

TABLE I  
ELECTRICAL PARAMETERS OF THE SAMPLE MOTOR DRIVE SYSTEM (REQUIRED INPUT DATA FOR MATLAB PROGRAMMING).

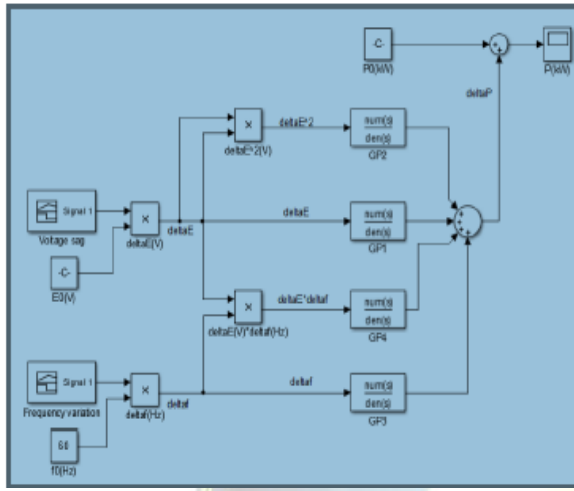
Induction Motor Parameters	Converter, inverter, DC parameters, PI speed controller
Nominal power 1500 HP	Diode forward voltage $V_{diode} = 1.3$ V
Nominal voltage $V_b = 2300$ V (rms)	DC bus capacitor $C_{dc} = 10000e-6$ F
Nominal frequency $f_{rated} = 60$ Hz	DC bus resistance $r_{dc} = 0$ $\Omega$
$R_s = 0.056$ $\Omega$ , $L_s = 0.001$ H	DC bus inductance $L_{dc} = 0$ H
$R_r = 0.037$ $\Omega$ , $L_r = 0.001$ H	Output frequency $f_{out} = 60$ Hz
$L_m = 0.0527$ H	PI speed controller Proportional gain
Inertia $J = 44.548$ Kg* m <sup>2</sup>	$K_{pm} = 9$
Nominal speed $n_{nom} = 1783$ rpm	PI speed controller Integral gain
Pole pairs $p = 2$	$K_{im} = 10$
Load torque $T_L = 1500$ Nm	
Target speed $n_{oper} = 1771$ rpm	
Power Source	
Rated voltage 480 V (rms)	
Rated frequency $f_g = 60$ Hz	
Commutation inductance $L_c$ including the phase-shifting transformer impedance = 1.2 mH	

### D. The Derived Dynamic Load Model for the Motor Drive System

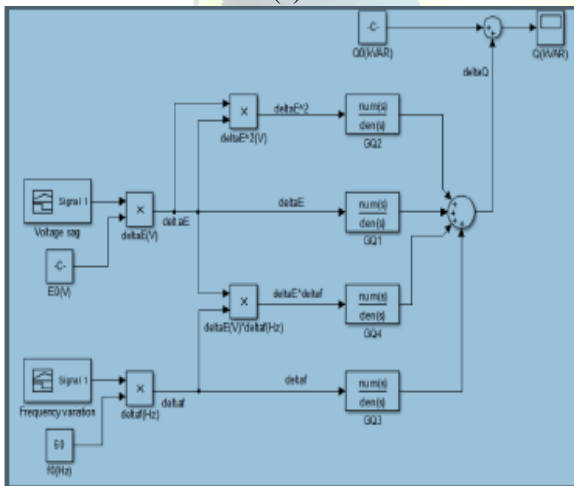
At the drive input, the real and reactive power at each power module are same and the total real power ( $P_{ac}$ ) and reactive power ( $Q_{ac}$ ) can be expressed by the power module number,  $\frac{n_{pulse}}{2}$ , multiplied by the real power and reactive power for each power

module as follows (for example, for an eighteen-pulse drive, the power module number is 9).

By combining differential equations of the converter, DC link, inverter, induction motor and the control system, and conducting linearization for all differential equations of the system, the equivalent dynamic model for the medium voltage motor system is



(a)



(b)

FIGURE.3 Simulink model and its schematic diagram based on the developed model for the sample system: (a) Simulink model for the real power P; (b) Simulink model for the reactive power Q; and (c) schematic diagram of the developed load model

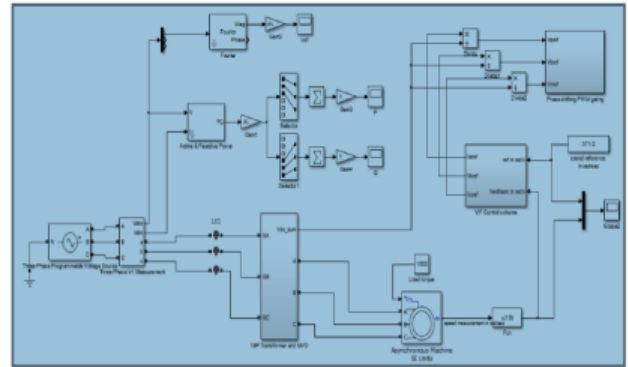


FIGURE.4 Detailed switching model for the sample system built using Simulink.

For an 18-pulse or a 24-pulse drive, just simply assign the pulse number n-pulse in (3) as 18 or 24 accordingly. The proposed modeling concept in the medium voltage motor drive systems can be used for large induction motor or synchronous motor applications.

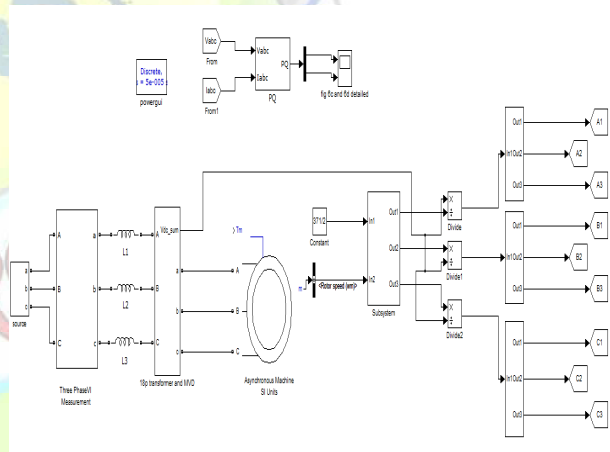


FIGURE.5 Block diagram of simulation

### III.FUZZY LOGIC CONTROLLER

In Fuzzy Logic Controller, basic control action is determined by a set of linguistic rules. Since the numerical variables are converted into linguistic variables, mathematical modeling of the system is not required in FC.

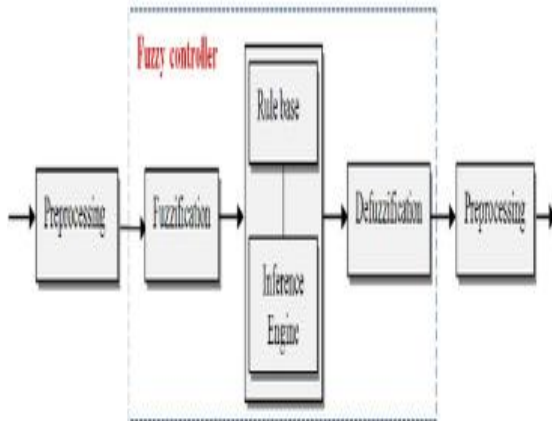


FIGURE.6 Fuzzy logic controller

The FLC comprises of three parts: Fuzzification, interference engine and defuzzification. The FLC is characterized as: mainly seven fuzzy sets for each input and output, Triangular membership functions for simplicity, Fuzzification using continuous universe of discourse, Implication using Mamdani's, 'min' operator and Defuzzification using the height method.

TABLE II: FUZZY RULES

Change in error	Error						
	NB	NM	NS	Z	PS	PM	PB
NB	PB	PB	PB	PM	PM	PS	Z
NM	PB	PB	PM	PM	PS	Z	Z
NS	PB	PM	PS	PS	Z	NM	NB
Z	PB	PM	PS	Z	NS	NM	NB
PS	PM	PS	Z	NS	NM	NB	NB
PM	PS	Z	NS	NM	NM	NB	NB
PB	Z	NS	NM	NM	NB	NB	NB

### A. FUZZIFICATION

Membership function values are assigned to the linguistic variables, using seven fuzzy subsets: NB (Negative Big), NM (Negative Medium), NS (Negative Small), ZE (Zero), PS (Positive Small), PM (Positive Medium), and PB (Positive Big). The Partition of fuzzy subsets and the shape of membership CE(k) E(k) function adapt the shape up to appropriate system. The value of input error and change in error are normalized by an input scaling

factor. In this system the input scaling factor has been designed such that input values are between -1 and +1. The triangular shape of the membership function of this arrangement presumes that for any particular E(k) input there is only one dominant fuzzy subset. The input error for the FLC is given as

$$E(k) = \frac{P_{ph(k)} - P_{ph(k-1)}}{V_{ph(k)} - V_{ph(k-1)}} \quad (21)$$

$$CE(k) = E(k) - E(k-1) \quad (22)$$

### B. INFERENCE METHOD

Several composition methods such as Max-Min and Max-Dot have been proposed in the literature. In this paper Min method is used. The output membership function of each rule is given by the minimum operator and maximum operator. Table II shows rule base of the FLC. [9] presented a short overview on widely used microwave and RF applications and the denomination of frequency bands. The chapter start outs with an illustrative case on wave propagation which will introduce fundamental aspects of high frequency technology.

### C. DEFUZZIFICATION

As a plant usually requires a non-fuzzy value of control, a defuzzification stage is needed. To compute the output of the FLC, „height” method is used and the FLC output modifies the control output. Further, the output of FLC controls the switch in the inverter. In UPQC, the active power, reactive power, terminal voltage of the line and capacitor voltage are required to be maintained. In order to control these parameters, they are sensed and compared with the reference values. To achieve this, the membership functions of FC are: error, change in error and output. The set of FC rules are derived from

$$u = -[\alpha E + (1-\alpha)C] \quad (23)$$

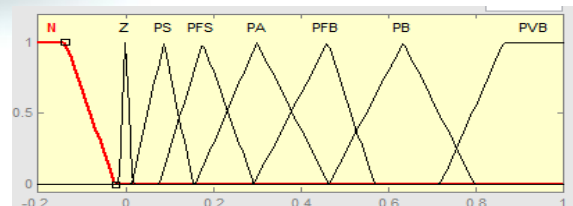


FIGURE.7 input error as membership functions

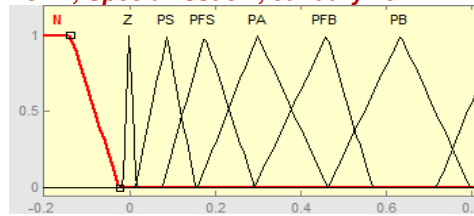


FIGURE.8 change as error membership functions

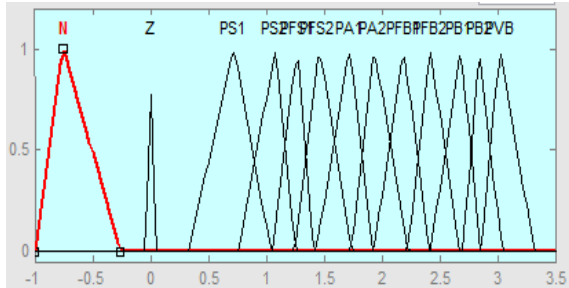


FIGURE.9 output variable Membership functions

Where  $\alpha$  is self-adjustable factor which can regulate the whole operation. E is the error of the system, C is the change in error and u is the control variable.

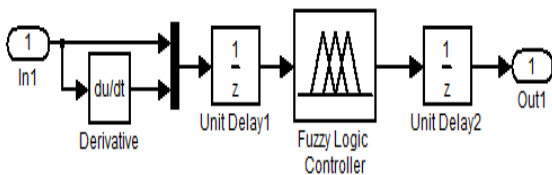


FIGURE.10 fuzzy logic controller in simulation

#### IV .VERIFICATION OF THE DEVELOPED DYNAMIC LOAD MODEL USING A CASE STUDY

##### A.THE SAMPLE SYSTEM

A case study is conducted using a sample medium voltage cascaded H-bridge M-level pulse width modulation inverter motor drive system to verify the developed model. The calculated model using the proposed method will be compared with a detailed switching model. Therefore, such a model can serve as a form of verification for the developed dynamic load model.

##### B.VERIFICATION OF VOLTAGE DEPENDENCE

To verify the voltage dependence characteristic of the pro- posed dynamic load model, a remote three-phase fault is applied to the drive input, which causes a 90% voltage sag in the detailed switching model. The fault starts from 14.4 s and is cleared at 14.65 s, and the frequency of the power source remains the

same. Dynamic responses of the two models for the 90% volt- age sag are shown in Fig. 11.

##### C.VERIFICATION OF FREQUENC DEPENDENCE

To verify the frequency dependence characteristic of the proposed dynamic load model, a frequency variation step- changed from 60 Hz to 55 Hz is applied at the power source in the detailed switching model. This frequency variation starts from 14.4 s and is cleared at 14.65 s.

It is interesting to note that a small voltage variation is caused by the frequency variation. Both frequency and voltage variations at the drive input in the detailed switching model are applied directly to the developed dynamic load model in order to compare dynamic responses of the two models under the same disturbances.

Dynamic responses of the two models subjected to the frequency variation are shown in Fig. 12. The comparison shows good agreement and similar tendency between the two models, which verifies the adequacy of the proposed model regarding the frequency dependence.

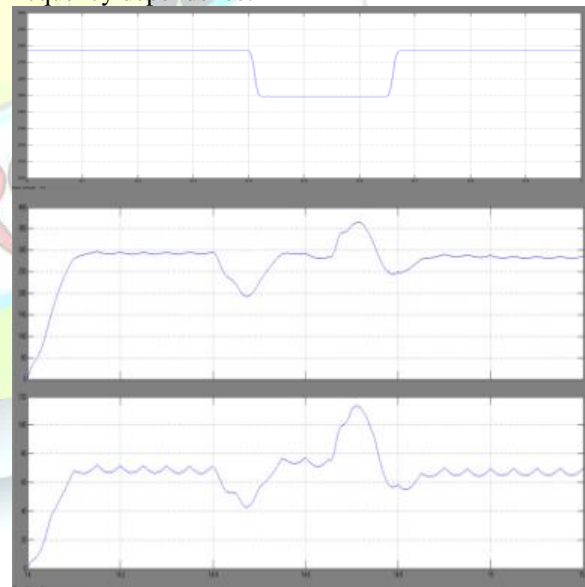


FIGURE.11 Dynamic response of the developed dynamic load model and the detailed switching model of the sample system when subjected to a 90% voltage sag: (a) voltage sag, (b) real power P, and (c) reactive power Q.

Fig. 12 indicates that the real power is not sensitive to frequency variations and remains the same during the frequency disturbance. However, the reactive power appears to be more sensitive to the frequency



variation, and the reactive power is reduced to a lower value during the frequency sag.

Based on the model verification, it is concluded that the proposed dynamic load model is able to confine major dynamic characteristics of the medium voltage cascaded H-bridge M-level inverter drive system and accurately determine its contribution to the power grid during disturbances in power system.

Therefore, it is an adequate model of this type of motor drive systems, and is suitable for power systems dynamic studies

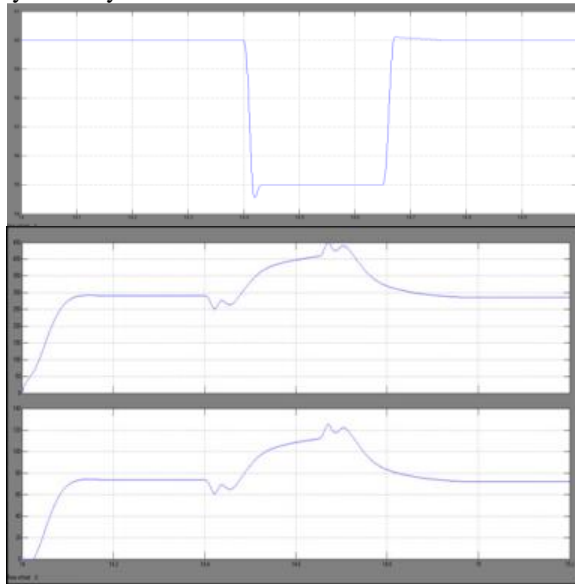


FIGURE.12 Dynamic response of the developed dynamic load model and the detailed switching model for a frequency variation: (a) frequency variation, (b) voltage variation, (c) real power P, and (d) reactive power Q.

#### V. SENSITIVITY STUDY

The sensitivity study of the designed model for the sample system in the case study is conducted to estimate the impact of the following three parameters on dynamic response characteristics: 1) parameters of the speed PI controller,  $K_p$  and  $K_i$ , for the voltage per Hz control; 2) the DC link capacitance  $C_{dc}$  inside each power module of the medium voltage drive; and 3) load torque  $TL$  of the induction motor.

Fig. 7 shows the dynamic response of the calculated model for a 90% voltage sag where the parameters of the speed PI controller ( $K_p$  and  $K_i$ ). The following three cases are considered: (1)  $K_p = 1:25$ , and  $K_i = 1:6$ ; (2)  $K_p = 9$ , and  $K_i = 10$ ; (3)  $K_p = 0:1$ , and  $K_i = 0:01$ . Other parameters are same as that listed in Table I. Case 2 with control parameters of

$K_p = 9$  and  $K_i = 10$  shows the best performance. The system is able to recover quickly after disturbances and reaches to previous steady-state values, which coincides with the detailed switching model response as shown in Fig. 11. However, Cases 1 and 3 do not have good performance during disturbances. Therefore, it is very important that proper control parameters for the speed PI controller are used in the calculated dynamic load model (such as  $K_p = 9$  and  $K_i = 10$ ), otherwise, the system will not be able to reach a steady-state after disturbances, and the simulation results will not match with the reality.

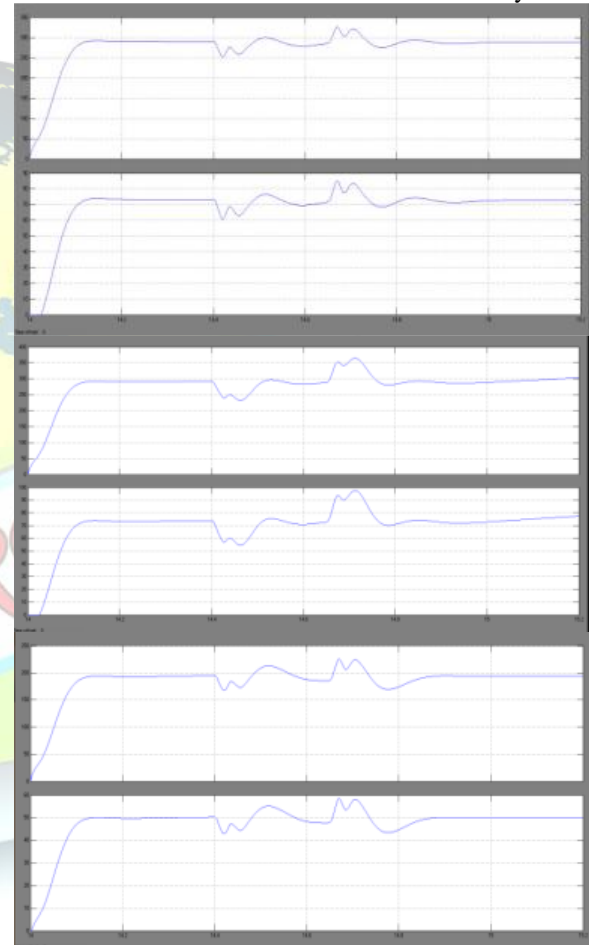


FIGURE.13 Dynamic response of the developed dynamic load model due to different speed controller parameters,  $K_p$  and  $K_i$ : (a) real power P and (b) reactive power Q.

The simulated dynamic response of the developed model with different DC link capacitance values  $C_{dc}$  inside a power module of the medium voltage drive when subjected to a 90% voltage sag are shown in Fig. 14. The  $C_{dc}$  values are 9200 micro farads, 10000 micro farads and 18000 micro farads. Other



parameters are same as that listed in Table I. It is found that increasing the DC link capacitance tends to increase the magnitude of dynamic transient for the real and reactive power. However, it has no effect on the steady-state values for the real and reactive power.

Three different load torques  $T_L$  are applied to the induction motor for the proposed dynamic model when subjected to a 90% voltage sag: 1000 Nm, 1500 Nm and 2000 Nm, which correspond to 17.3%, 25.9% and 34.5% loading of the motor, respectively. Other parameters are same as that listed in Table I.

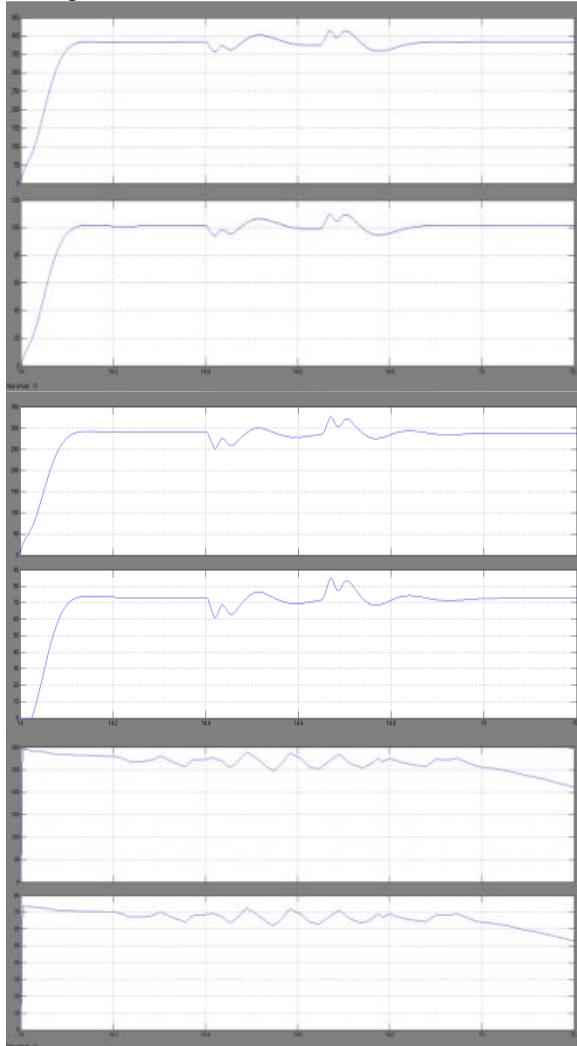


FIGURE.14 Dynamic response of the developed dynamic model due to different DC link capacitance  $C_{dc}$  of each power module inside the medium voltage drive: (a) real power P and (b) reactive power Q

The simulated dynamic responses of the developed model in this case are shown in Fig. 15. It is found

that the load factor of the motor has significant effect on both steady-state and dynamic responses for the real and reactive power.

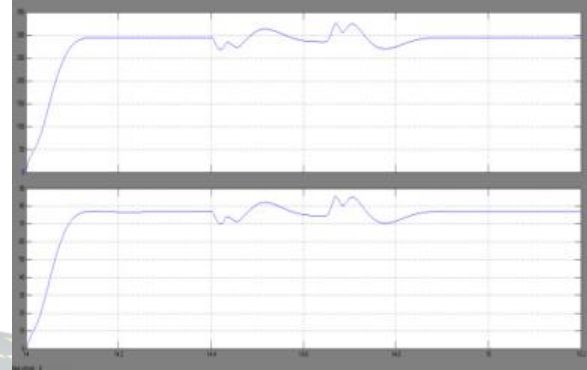


FIGURE.15 Dynamic response of the developed dynamic model due to different load torque of the induction motor TL: (a) real power P and (b) reactive power Q.

#### V.CONCLUSION

The dynamic load model for medium voltage cascaded H-bridge M-level pulse-width- modulated (PWM) inverter motor drive system is developed in this paper, which is derived using an analytical method called the linearization approach. Fuzzy controller has a lot of parameters. The most important is to make a good choice of rule base and parameters of membership functions. The accuracy of the proposed model is verified by a case study using a sample medium voltage motor drive system. Here we are using the fuzzy controller compared to other controllers. The DVR and control strategy successfully interrupts the downstream fault currents and improves the efficiency of the system. The developed dynamic load model for medium voltage motor drive system is expressed by 7th order transfer functions with both voltage dependence and frequency dependence is considered. This proposed model can be inserted into large scale power system simulation software for power system dynamic studies, and the medium voltage cascaded H-bridge multi-level inverter drive and induction motor systems, which is suitable for power system dynamic studies, is proposed is proposed.

#### REFERENCES

- [1] IEEE Task Force on Load Representation for Dynamic Performance, "Load representation for dynamic performance analysis [of power systems]," IEEE Trans. Power Syst., vol. 8, no. 2, pp. 472-482, May 1993.
- [2] IEEE Task Force on Load Representation for Dynamic Performance, "Standard load models for



power ow and dynamic performance simulation," IEEE Trans. Power Syst., vol. 10, no. 3, pp. 13021313, Aug. 1995.

[3] A. Merdassi, L. Gerbaud, and S. Bacha, "A new automatic average modelling tool for power electronics systems," in Proc. IEEE Power Electron. Specialists Conf. (PESC), Jun. 2008, pp. 34253431.

[4] J. Sun and H. Grotstollen, "Averaged modelling of switching power converters: Reformulation and theoretical basis," in Proc. IEEE 23rd Annu. Power Electron. Specialists Conf. (PESC), vol. 2. Jun./Jul. 1992, pp. 11651172.

[5] S. Cuk and R. D. Middlebrook, "A general unified approach to modelling switching-converter power stages," in Proc. IEEE Annu. Power Electron. Specialists Conf. (PESC), Jun. 1976, pp. 1831.

[6] A. Griffo, J. B. Wang, and D. Howe, "State-space average modelling of eighteen-pulsed diode rectifier," in Proc. 3rd Int. Conf. Sci. Comput. Comput. Eng. (IC-SCCE), Jul. 2008, pp. 18.

[7] T. A. Meynard, M. Fadel, and N. Aouda, "Modeling of multilevel converters," IEEE Trans. Ind. Electron., vol. 44, no. 3, pp. 356364, Jun. 1997.

[8] A. Uan-Zo-li, R. P. Burgos, F. Lacaux, F. Wang, and D. Boroyevich, "Assessment of multipulse converter average models for stability studies using a quasistationary small-signal technique," in Proc. 4th Int. Power Electron. Motor Control Conf., vol. 3. Aug. 2004, pp. 16541658.

[9] Christo Ananth, [Account ID: AORZMT9EL3DL0], "A Detailed Analysis Of Two Port RF Networks - Circuit Representation [RF & Microwave Engineering Book 1]", Kindle Edition, USA, ASIN: B06XQY4MVL, ISBN: 978-15-208-752-1-7, Volume 8, March 2017, pp:1-38.

[10] A. Emadi, A. Khaligh, C. H. Rivetta, and G. A. Williamson, "Constant power loads and negative impedance instability in automotive systems: Denition, modeling, stability, and control of power electronic converters and motor drives," IEEE Trans. Veh. Technol., vol. 55, no. 4, pp. 11121125, Jul. 2006.

[11] P. C. Krause, O. Wasynczuk, and S. D. Sudhoff, Analysis of Electric Machinery and Drive Systems, 2nd ed. Piscataway, NJ, USA: IEEE Press, 2002.

#### PATHI HOLY RANI



Completed B.Tech in Electrical & Electronics Engineering in 2015 from

JNTUUNIVERSITY, HYDERABAD and Pursuing M.Tech from ANURAG Group of Institutions(Formerly known as CVSR College of Engineering(Autonomous))Affiliated to JNTUH, Hyderabad, Telangana, India. Area of interest includes Power Electronics.

E-mail id: holyrani45@gmail.com

#### B.CHANDRA SEKHAR REDDY



Completed B.Tech in Electrical & Electronics Engineering in 2008 from JNTUH, Hyderabad and M.Tech in Electrical Power System Electronics in 2012 from

St'Marys College of Engineering and Technology Affiliated to JNTUH, Hyderabad. Working as Assistant Professor at ANURAG Group of Institutions(Formerly known as CVSR College of Engineering(Autonomous))Affiliated to JNTUH, Hyderabad, Telangana, India. Area of interest includes **Electrical Power System, power electronics, electrical drives control.**

E-mail id: Chandrashekaree@cvsr.ac.in